NeuroLink: Bridging Weak Signals in Neuronal Imaging with Morphology Learning

Haiyang Yan[1,2], Hao Zhai[1,2], Jinyue Guo[1,3], Linlin Li[1], and Hua Han[1,2(✉)]

[1] Laboratory of Brain Atlas and Brain-inspired Intelligence, Key Laboratory of Brain Cognition and Brain-inspired Intelligence Technology, Institute of Automation, Chinese Academy of Sciences, Beijing 100190, China
{hua.han}@ia.ac.cn

[2] School of Future Technology, University of Chinese Academy of Sciences, Beijing 101408, China

[3] School of Artificial Intellengace, University of Chinese Academy of Sciences, Beijing, China

Abstract. Reconstructing neurons from large-scale optical microscope images is a challenging task due to the complexity of neuronal structures and extremely weak signals in certain regions. Traditional segmentation models, built on vanilla convolutions and voxel-wise losses, struggle to model long-range relationships in sparse volumetric data. As a result, weak signals in the feature space get mixed with noise, leading to interruptions in segmentation and premature termination in neuron tracing results. To address this issue, we propose NeuroLink to add continuity constraints to the network and implicitly model neuronal morphology by utilizing multi-task learning methods. Specifically, we introduce the Dynamic Snake Convolution to extract more effective features for the sparse tubular structure of neurons and propose a easily implementable morphology-based loss function to penalize discontinuous predictions. In addition, we guide the network to leverage the morphological information of the neuron for predicting direction and distance transformation maps of neurons. Our method achieved higher recall and precision on the low-contrast Zebrafish dataset and the publicly available BigNeuron dataset. Our code is available at https://github.com/Qingjia0226/NeuroLink.

Keywords: Neuronal segmentation · Multi-Task learning · Neuronal morphology · Fluorescence microscopy

1 Introduction

With the development of imaging technology, neuroscientists are able to obtain large-scale optical neuronal images for studying cell morphologies and neuronal circuits [1]. 3D neuron reconstruction (*i.e.*, neuron tracing) aims to obtain a digitized tree representation of neurons from these images. Classic rule-based neuron tracing algorithms such as local method neuTube [5] , global method APP2 [24], meta method ENT [20] excel in processing high-quality single-neuron images, yet they encounter limitations when faced with long projection axonal branches

[12]. However, in whole-brain imaging, the uneven distribution of fluorescent labels in neurons frequently leads to discontinuity and weakened filament signals [27]. Neurons show a certain morphological structure at the global level, but can only present sparse and weak signals at the local level. Segmenting neurons on fluoroscopic images is therefore a unique and intractable task even within the broader field of computer vision.

To denoise the images and enhance weak signals, many methods[26, 21, 11, 8] use Convolutional Neural Network (CNN) for image segmentation as a preprocessing step. During training, they simply utilize Dice and Binary CrossEntropy (BCE) loss, which lack constraints on the morphological structure of neurons. The subsequent work focus on three directions for the retrieval of lost signal and correctness of the topology: designing topology-based loss functions, modeling neuron morphology, and post-processing segmentation results. Certain works punish different topological structures using loss functions like discrete Morse theory[6] and persistent homology[4], but their theoretical and computational methods are intricate and need to be carefully designed to assure differentiability. [3] compare the neuron segmentation results with existing morphologies for adversarial learning to learn the neuron morphology, but the reconstructed target dataset and existing morphologies may not follow the same distribution. [22] and [27] introduce multi-task learning, respectively predicting Flux features and distances to the centerline to improve neuron segmentation, but the tasks are relatively singular and do not utilize broader features of neurons. Some works[7, 29] use heuristic post-processing algorithms to repair predicted results of fractures to restore neuron morphology, but their rule applicability is limited and challenging to generalize to large-scale data. Other methods, such as derivative truncated gamma transformation and adding penalties for false negative voxels[13], mitigate false negative issues but do not consider neuron morphology.

In this paper, we propose a new neural segmentation method called NeuroLink, which guides the network to learn the morphological features of neurons in a spatially continuous manner to improve the segmentation in regions with weak signal. Specifically, we introduce Dynamic Snake Convolution (DSC) to the low-level feature map and design multiple convolutional kernel offsets to extract multi-perspective features. The convolutional kernels adaptively fit the tubular or branching structures of neurons at different positions, which helps maintain the local continuity. In addition, we propose a Weighted Local Connectivity (WLC) loss to detect long-range false negative segmentation fragments by utilizing multiple dilation operation and applying weighted penalties. The WLC loss also penalizes incorrect connections to assist the network in determining the neuronal connectivity. Furthermore, we design a multi-task learning approach that guides the network to learn relevant representations of morphology by predicting the local orientation of neurons and the distance to the central line. We conducted experiments on the Gold166 and Zebrafish datasets to validate the effectiveness of our algorithm.

The main contributions of our work are summarized as follows: (1) We introduce DSC into U-Net and propose the WLC loss to improve the continuity

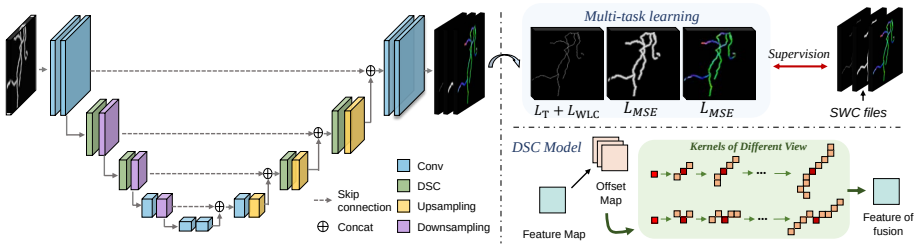

Fig. 1. The framework of NeuroLink. The green blocks in the second and third layers of the network correspond to the DSC module. The network produces outputs with five channels, comprising probability map, distance transformation map, and three components of direction vector.

of network predictions. (2) We design a novel multi-task learning approach that leverages distance and orientation predictions to steer the model towards acquiring representations of neuron morphology. (3) Experiments on the Gold166 and Zebrafish datasets demonstrate that our method significantly enhances the recall and F1 score of neuron tracking in low-contrast images.

2 Method

The framework of our method is illustrated in the Fig.1, which adopts a classic encoder-decoder architecture. The features extracted by DSC that better match the tubular structure of neurons, along with the collaborative constraints of multi-task learning, enable the model to acquire stronger morphological characteristics of neurons.

2.1 DSC Module: To Learn Better Local Feature

Neurons appear fragile and curved under optical microscope. Capturing effective features from such sparse structures poses a challenge for traditional convolutional kernels. Inspired by the DSC[16] which dynamically adjusts the convolutional receptive field to accommodate slender structures, we explored the optimal implementation of DSC and found it to be more effective on low-dimensional feature maps of neuron images. We then inserted it into the 2nd and 3rd layers of the U-Net. The process by which the DSC module obtains the shape of the convolution is depicted in Fig.1. We start by employing a $3\times3\times3$ convolution to predict an offset map of the same size as the input feature map. At each location on the feature map, the convolution kernel is centered, and by accumulating the values in the offset map, it extends to both ends. To address complex branching structures, we extract features from multiple perspectives at each position and then fuse them together.

To better guide the learning of displacement patterns by DSC, we propose a novel data augmentation method. By eroding local regions of the original image

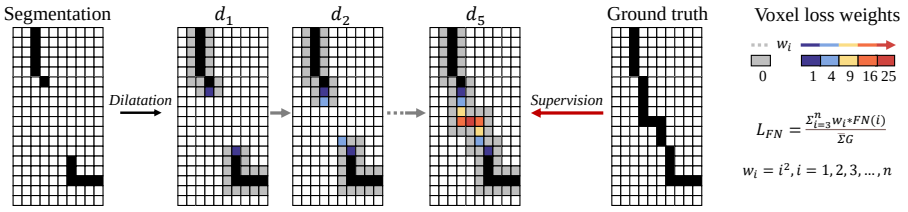

Fig. 2. A toy example of l_{FN}. We identify false negative voxels sequentially through dilation and apply weighted penalties.

to simulate weak signals resulting from the uneven distribution of fluorescence signals in imaging, we force the network to utilize neuron morphology information to make predictions at locations of fluorescence signal discontinuities. We randomly select positive sample points and perform erosion operations three times in a $20 \times 20 \times 10$ region centered at each point in the original image.

2.2 WLC Loss: To Learn Long-range Connectivity

DSC contributes to improving short-range continuity in neuron segmentation; however, it does not prevent the lost of large segmentation of neurons. In this section, we propose WLC loss, which complements DSC by penalizing longer false-negative predictions.

A naive approach to dealing with a long missing segmentation in a neuron branch is binary search method. This involves retrieving a portion in the middle of the lost parts, gradually filling in the gaps, and finally connecting two segments together. Neuron tracking methods can also be facilitated by splitting a big gap into smaller gaps. This inspires us to assign higher penalty weights to false-negative voxels that are morphologically further away from the prediction. Dilation procedures may be used to carry out the aforementioned concept. Fig. 2 shows the schematic representation of the complete procedure.

Denote the dilation operator as $\mathbf{d}$, the segmentation result as S. By multiplying $\mathbf{d}(S) - S$ with the ground truth G, false-negative voxels F that are one voxel away from S can be obtained. We merge F into S and continue with dilation to sequentially obtain false-negative voxels along the neurons. We perform the above operations n times and apply penalty weight i^α $(\alpha > 1)$ for the $F(i)$ acquired from the i-th operation in order to penalize F that are morphologically farther from the S. Consequently, we obtain the expression for l_{FN} :

$$l_{FN} = \frac{\sum_{i=3}^{n} i^\alpha ||G \cdot (\mathbf{d}(s_i) - s_i)||_1}{\sum G}, \tag{1}$$

where s_i represents the segmentation result obtained after merging the false-negative voxels from the first i iterations. To eliminate the influence of the neuron radius, we ignore the voxels obtained from the first two operations.

Meanwhile, to suppress false-positive connections between neurons that are close to each other but belong to different branches, we design the false positive loss l_{FP} to penalize such erroneous connections.

$$l_{FP} = \frac{\sum_{i=3}^{n}(n-i+3)^{\alpha}||S \cdot (\mathbf{d}(g_i) - g_i)\,||_1}{\sum S}. \tag{2}$$

WLC loss is the weighted sum of the l_{FN} and l_{FP}:

$$L_{WLC} = \beta l_{FN} + (1-\beta) l_{FP}. \tag{3}$$

2.3 Multiple Tasks: Learning Local Shape and Direction

By designing multiple tasks, we guide the network to utilize information from a larger receptive field to predict relevant labels, enabling the model to learn intrinsic features related to neuron morphology and structure.

Voxel Classification. The neuron annotation may lack radius information or contain inaccuracies in the provided radius information. Segmentation ground truth is often generated through certain approximations. In order to reduce the inaccuracies caused by approximations and address extreme class-imbalance, We utilize the Tversky loss[17] to further emphasize the recall of the segmentation results. The formula is as follows:

$$L_T = \frac{\sum_{i=1}^{N} p_{0i} g_{0i}}{\sum_{i=1}^{N} p_{0i} g_{0i} + (1-\gamma)\sum_{i=1}^{N} p_{0i} g_{1i} + \gamma \sum_{i=1}^{N} p_{1i} g_{0i}}, \tag{4}$$

where p_{0i} and p_{1i} is the probability of voxel i be a neuron and background respectively. g_{0i} is 1 for a neuron voxel and 0 for background and vice verse for the g_{1i}. N is the total number of voxels.

Distance Transform Map. We first compute the Euclidean distance transform map $T(p)$[19]. Instead of using Gaussian kernel [27] decaying rapidly, we propose to generate label through linear decay. The label is defined as follows:

$$t = \begin{cases} 1 - \frac{T(p)}{R} & \text{for } T(p) < R \\ 0 & \text{otherwise} \end{cases}. \tag{5}$$

The Mean Squared Error (MSE) is implemented between the predicted and the target distance transform maps, which can be represented as:

$$L_{dis} = \frac{\sum_i [m_i - t_i]^2}{N}, \tag{6}$$

where m_i is the predicted map at voxel i and t_i is the voxel value in the corresponding target distance transform map.

Direction. In addition to assisting the network in comprehending neuronal morphology, the prediction of direction can also be utilized for post-processing[29, 2, 26]. For point $P_i(x_1, y_1, z_1)$ on the centerline, there is a unique parent node

$P_{parent}(x_2, y_2, z_2)$ in the 26-neighborhood. We define the tangential vector direction at point P_i as $\boldsymbol{\Delta_i} = \frac{(x_1-x_2, y_1-y_2, z_1-z_2)}{\sqrt{(x_1-x_2)^2+(y_1-y_2)^2+(z_1-z_2)^2}}$. The average direction vector of the surrounding 5 points is used as the label $\boldsymbol{\Delta}$.

Using MSE loss to penalize the non-collinearity between the ground truth direction $\boldsymbol{\Delta}_g$ and the predicted direction$\boldsymbol{\Delta}_p$:

$$L_{dir} = \frac{\sum_i \left[\min\left[(\boldsymbol{\Delta}_g - \boldsymbol{\Delta}_p)^2, (\boldsymbol{\Delta}_g + \boldsymbol{\Delta}_p)^2\right]\right]}{N}. \tag{7}$$

The total loss is the sum of all losses in multi-task training:

$$L = L_T + L_{WLC} + L_{dir} + L_{dis}. \tag{8}$$

3 Experiments

3.1 Datasets and Evaluation Metrics

Gold166. The Bigneuron[14] project consists of images from various laboratory environments, different species, and varying sizes. The Gold166 dataset, comprising 166 representative neurons from Bigneuron with expert annotations, is commonly utilized for algorithm testing. Due to the significant differences within Gold166, we firstly select 28 images for training and 75 images for testing as[22]. For the second experiment, we randomly choose a ratio of 5:2:3 for training, validation, and testing for all images.

Zebrafish Dataset. The zebrafish dataset comprises confocal microscopy images of 6-day-old zebrafish larvae, with size of around $1000 \times 2000 \times 250$ voxels and resolution of $0.5 \times 0.5 \times 1\ \mu m/voxel$. The dataset is characterized by small cell body regions, numerous long-range axons and weak signals. We randomly select 61 images for training, 13 for validation and 29 for testing.

Evaluation Metrics. We use the most widely used Precision (PRE), Recall (REC) and F1 measure as primary evaluation metric. A point within 4 voxels to the ground truth was classified as a true point. Besides, the Structural Distance (SD) and substantial spatial distance (SSD) metric[15] is used to evaluate the distance between the target neuron nodes and the reconstructed neuron nodes. Miss-Extra-Scores (MES)[25] is calculated to measure the expected parts of the centerline and the undesired components.

3.2 Implementation Details

The parameters α, β and n of the proposed WLC loss are set as 2, 0.5 and 12 respectively. In Eq.4 we set $\gamma = 0.7$. In Eq.5 we choose R=10. We leverage the operation in [18] to facilitate rapid and efficient dilation in PyTorch.

For data augmentation, we use image flipping, random rotation, random changes in brightness and contrast, misalignment, and the erosion operation around neurons. The tracking algorithm APP2[24] is applied to the weighted

image with a segmentation-to-original image ratio of 4:1 to obtain the tracking results. Subsequently, the nodes are resampled to the 26-neighborhood connectivity and compared with the ground truth.

An AdamW optimizer was employed with a cosine decay learning rate scheduler and linear warmup of 1000 iterations. The batch size and patch size are set to 4 and 237 × 237 × 47. LeakyReLU and Group Normalization are applied. Our method was implemented in PyTorch 1.12 and trained on Tesla V100 GPU.

3.3 Evaluation on Gold166 dataset

Table 1. Quantitative results on 75 neurons in Gold166 dataset.

	Method	SD↓	SSD↓	PRE↑	REC↑	F1↑	MES↑
classic	APP2[24]	10.614	17.311	0.795	0.731	0.765	0.592
	ENT[20]	12.565	16.809	0.507	0.512	0.497	0.320
	FMST[28]	7.623	14.108	0.673	0.663	0.664	0.506
	ON[9]	7.946	13.787	0.590	0.599	0.589	0.473
deep learning	TopNet[10]	7.080	11.530	0.709	0.563	0.624	0.408
	tubular flux model[22]	5.045	12.956	0.826	0.747	0.781	0.616
	our base	9.362	12.242	0.901	0.914	0.902	0.753
	+mT	6.292	8.954	0.901	0.915	0.901	0.754
	+mT+DSC	3.338	6.265	0.904	**0.935**	0.911	**0.762**
	+mT+WLC	3.016	5.960	0.912	0.929	**0.915**	0.760
	NeuroLink(Ours)	**2.906**	**5.817**	**0.913**	0.929	**0.915**	0.760

mT: multi-Task, our base: vanilla 3D U-Net.

Table 2. Results of all categories of neurons in Gold166 dataset.

Method	PRE↑	REC↑	F1↑
Li-2017[11]	0.7073	0.5197	0.5979
Huang-2020[8]	0.5964	0.508	0.5487
MP-NRGAN[3]	**0.7117**	0.5563	0.6245
SGSNET[27]	0.6920	0.5047	0.5837
NRTR[23]	0.7044	0.6533	0.6779
NeuroLink(Ours)	0.6717	**0.7657**	**0.7156**

Table 1 presents the quantitative results comparing the different implementations of our method with popular methods in Gold166 dataset. Our method not only tracked more subtle signals significantly improving the recall but also get the smaller SD, indicating reconstruction results closer to the ground truth

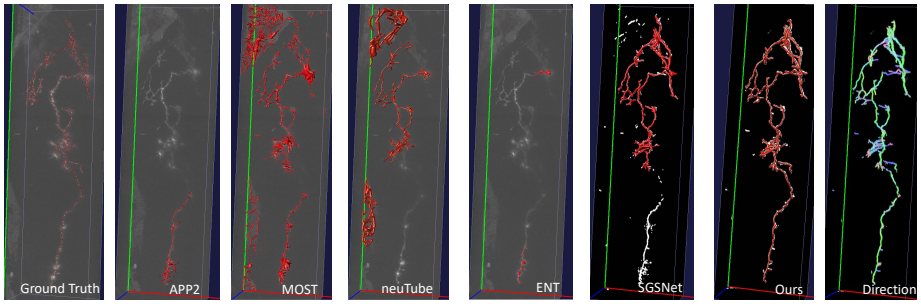

Fig. 3. Visualization of ground truth and neuron tracing results on Zebrafish dataset by different algorithms as indicated. The reconstruction results of deep learning-based method are displayed on its segmentation. We also show the predicted direction map of NeuroLink, with directions in the x,y,z axes represented by blue, green, and red.

annotations. Experimental results indicate that multi-task method 3D tubular flux model[22] and our multi-task strategy improved SD and SSD performance. DSC effectively increase the recall rate, but the continuous convolution kernels erroneously connect irrelevant structures around the neurons, reducing precision. The incorporation of WLC loss address this issue, achieving the best results.

Table 2 shows the performance of popular deep learning-based methods on the entire Gold166 dataset. Our method achieved higher recall and F1 scores while maintaining similar precision.

3.4 Ablation study on Zebrafish Dataset

To validate the effectiveness and optimal implementation of our module, we conducted experiments on the Zebrafish dataset. Figure 3 presents the results on a challenging neuron image from Zebrafish dataset, showing that representative classic methods exhibit significant errors on such low-contrast, weak-signal neuron image. Outstanding deep learning methods, such as SGSNet[27], are imperfect in weak signal areas, resulting in premature termination of neuron tracing. Our method obtain the complete morphology of neurons.

Table 3 presents the quantitative results of different methods. The experiment shows multi-task method can improve the accuracy of network predictions, but it do not enhance recall. WLC loss reduces the missing of large neuron segmentation, improving the recall by 10%. Besides, implementing DSC in the 2nd and 3rd layers of U-Net yields better performance than in the 4th and 5th layers. Our method improved the F1 score by 25.6% compared to APP2.

4 Conclusion

In this paper, we aim to mitigate the discontinuous segmentation caused by weak signals by introducing DSC and proposing WLC loss to impose constraints. Additionally, we propose a novel multi-task learning approach to fully leverage

Table 3. Performance on Zebrafish dataset.

Method	SD↓	SSD↓	PRE↑	REC↑	F1↑	MES↑
APP2	26.744	35.443	0.793	0.677	0.678	0.587
base	31.303	34.962	0.869	0.814	0.836	0.809
+mT	22.801	30.916	0.983	0.775	0.825	0.756
+WLC+mT	11.553	20.114	0.981	0.874	0.912	0.874
+DSC-23+mT	7.595	17.935	0.982	0.889	0.928	0.889
+DSC-45+WLC+mT	14.281	22.683	0.978	0.857	0.893	0.855
Ours	**6.880**	**16.253**	**0.984**	**0.897**	**0.934**	**0.899**

mT: multi-Task, base: vanilla 3D U-net,
DSC-23: DSC in 2nd and 3rd layers, DSC-45: DSC in 4th and 5th layers.

the information of neurons and learn morphology features. NeuroLink exhibits significant advantages on different datasets. This approach of incorporating continuity priors and modeling morphology of the target can also inspire other tasks in computer vision that involve segmenting continuous and sparse objects.

Acknowledgments. This work was supported by grants from the STI 2030-Major Projects (2021ZD0204500, 2021ZD0204503 to L.L.), STI 2030-Major Projects (2022ZD0211900, 2022ZD0211902 to L.S.). We are grateful for the Zebrafish dataset provided by Jiulin Du and Xufei Du from Institute of Neuroscience, Center for Excellence in Brain Science and Intelligence Technology, Chinese Academy of Sciences.

Disclosure of Interests. The authors have no competing interests to declare that are relevant to the content of this article.

References

[1] Runze Chen et al. "Deep learning in mesoscale brain microscopy image analysis: A review". In: *Computers in Biology and Medicine* (2023), p. 107617.

[2] Weixun Chen et al. "Deep-learning-based automated neuron reconstruction from 3D microscopy images using synthetic training images". In: *IEEE Transactions on Medical Imaging* 41.5 (2021), pp. 1031–1042.

[3] Xuejin Chen et al. "Weakly supervised neuron reconstruction from optical microscopy images with morphological priors". In: *IEEE Transactions on Medical Imaging* 40.11 (2021), pp. 3205–3216.

[4] Andac Demir, Elie Massaad, and Bulent Kiziltan. "Topology-Aware Focal Loss for 3D Image Segmentation". In: *Proceedings of the IEEE/CVF Conference on Computer Vision and Pattern Recognition*. 2023, pp. 580–589.

[5] Linqing Feng, Ting Zhao, and Jinhyun Kim. "neuTube 1.0: a new design for efficient neuron reconstruction software based on the SWC format". In: *eneuro* 2.1 (2015).

[6] Xiaoling Hu et al. "Topology-aware segmentation using discrete Morse theory". In: *arXiv preprint arXiv:2103.09992* (2021).

[7] Qing Huang et al. "Minimizing probability graph connectivity cost for discontinuous filamentary structures tracing in neuron image". In: *IEEE Journal of Biomedical and Health Informatics* 26.7 (2022), pp. 3092–3103.

[8] Qing Huang et al. "Weakly supervised learning of 3D deep network for neuron reconstruction". In: *Frontiers in Neuroanatomy* 14 (2020), p. 38.

[9] Michael Kerschnitzki et al. "Architecture of the osteocyte network correlates with bone material quality". In: *Journal of bone and mineral research* 28.8 (2013), pp. 1837–1845.

[10] Deepak Keshwani et al. "TopNet: Topology preserving metric learning for vessel tree reconstruction and labelling". In: *Medical Image Computing and Computer Assisted Intervention–MICCAI 2020: 23rd International Conference, Lima, Peru, October 4–8, 2020, Proceedings, Part VI 23*. Springer. 2020, pp. 14–23.

[11] Rongjian Li et al. "Deep learning segmentation of optical microscopy images improves 3-D neuron reconstruction". In: *IEEE transactions on medical imaging* 36.7 (2017), pp. 1533–1541.

[12] Yufeng Liu et al. "Neuron tracing from light microscopy images: automation, deep learning and bench testing". In: *Bioinformatics* 38.24 (2022), pp. 5329–5339.

[13] Yufeng Liu et al. "Tracing weak neuron fibers". In: *Bioinformatics* 39.1 (2023), btac816.

[14] Hanchuan Peng et al. "BigNeuron: large-scale 3D neuron reconstruction from optical microscopy images". In: *Neuron* 87.2 (2015), pp. 252–256.

[15] Hanchuan Peng et al. "V3D enables real-time 3D visualization and quantitative analysis of large-scale biological image data sets". In: *Nature biotechnology* 28.4 (2010), pp. 348–353.

[16] Yaolei Qi et al. "Dynamic snake convolution based on topological geometric constraints for tubular structure segmentation". In: *Proceedings of the IEEE/CVF International Conference on Computer Vision*. 2023, pp. 6070–6079.

[17] Seyed Sadegh Mohseni Salehi, Deniz Erdogmus, and Ali Gholipour. "Tversky loss function for image segmentation using 3D fully convolutional deep networks". In: *International workshop on machine learning in medical imaging*. Springer. 2017, pp. 379–387.

[18] Suprosanna Shit et al. "clDice-a novel topology-preserving loss function for tubular structure segmentation". In: *Proceedings of the IEEE/CVF Conference on Computer Vision and Pattern Recognition*. 2021, pp. 16560–16569.

[19] Amos Sironi et al. "Multiscale centerline detection". In: *IEEE Transactions on Pattern Analysis and Machine Intelligence* 38.7 (2015), pp. 1327–1341.

[20] Ching-Wei Wang et al. "Ensemble neuron tracer for 3D neuron reconstruction". In: *Neuroinformatics* 15 (2017), pp. 185–198.

[21] Heng Wang et al. "Voxel-wise cross-volume representation learning for 3d neuron reconstruction". In: *Machine Learning in Medical Imaging: 12th International Workshop, MLMI 2021, Held in Conjunction with MICCAI 2021, Strasbourg, France, September 27, 2021, Proceedings 12*. Springer. 2021, pp. 248–257.

[22] Xuan Wang et al. "A 3D tubular flux model for centerline extraction in neuron volumetric images". In: *IEEE Transactions on Medical Imaging* 41.5 (2021), pp. 1069–1079.

[23] Yijun Wang et al. "NRTR: Neuron reconstruction with transformer from 3D optical microscopy images". In: *IEEE Transactions on Medical Imaging* (2023).

[24] Hang Xiao and Hanchuan Peng. "APP2: automatic tracing of 3D neuron morphology based on hierarchical pruning of a gray-weighted image distance-tree". In: *Bioinformatics* 29.11 (2013), pp. 1448–1454.

[25] Jun Xie et al. "Anisotropic path searching for automatic neuron reconstruction". In: *Medical image analysis* 15.5 (2011), pp. 680–689.

[26] Bo Yang et al. "Neuron image segmentation via learning deep features and enhancing weak neuronal structures". In: *IEEE Journal of Biomedical and Health Informatics* 25.5 (2020), pp. 1634–1645.

[27] Bo Yang et al. "Structure-guided segmentation for 3D neuron reconstruction". In: *IEEE transactions on medical imaging* 41.4 (2021), pp. 903–914.

[28] Jian Yang et al. "FMST: an automatic neuron tracing method based on fast marching and minimum spanning tree". In: *Neuroinformatics* 17 (2019), pp. 185–196.

[29] Fuhao Yu et al. "Automatic repair of 3-D neuron reconstruction based on topological feature points and an MOST-based repairer". In: *IEEE Transactions on Instrumentation and Measurement* 70 (2020), pp. 1–13.